Organic nanodots for multiphotonics: synthesis and photophysical studies†

Olivier Mongin,[a] Anna Pla-Quintana,[b] Francesca Terenziani,[ac] Delphine Drouin,[a] Céline Le Droumaguet,[a] Anne-Marie Caminade,[b] Jean-Pierre Majoral*[b] and Mireille Blanchard-Desce*[a]

Received (in Montpellier, France) 15th February 2007, Accepted 31st May 2007
First published as an Advance Article on the web 8th June 2007
DOI: 10.1039/b702452p

Organic nanodots based on the gathering of an exponentially increasing number of two-photon fluorophores on a dendritic platform of controlled size and symmetry represent a promising non-toxic alternative to quantum dots for (bio)imaging purposes. This modular route offers a number of advantages in terms of versatility but also raise a number of questions to be addressed. In particular, possible interactions between fluorophores, due to confinement effects, have to be taken into account. With this aim in mind we have investigated and compared the photophysical and two-photon absorption (TPA) properties of two series of organic nanodots of different geometries: spherical-like organic nanodots derived from a dendritic scaffold built from a cyclotriphosphazene core and dumbbell-like organic nanodots derived from a dendritic scaffold built from an elongated rod-like chromophore. The study provides evidence that the different topology and nature of the dendritic architecture lead to significant changes in photoluminescence characteristics as well as to subtle variations of the TPA efficiency. As a result, the dumbbell-like nanodots although less promising in terms of two-photon induced fluorescence (due to partial quenching of fluorescence efficiency) also demonstrate that improvement of the TPA efficiency can be achieved by playing on the nature and topology of the dendritic scaffold of the nanodots.

Introduction

Molecular two-photon absorption (TPA) has attracted a lot of interest over the last decade owing to its applications in various fields including spectroscopy,[1,2] three-dimensional optical data storage,[3–5] microfabrication,[6–8] laser up-conversion,[9,10] high-resolution three-dimensional imaging of biological systems,[11–13] and photodynamic therapy.[14] Among these, two-photon-excited fluorescence (TPEF) has gained widespread popularity in the biology community and given rise to the technique of two-photon laser scanning fluorescence microscopy.[11–13] Using a two-photon excitation process (*i.e.* a nonlinear process involving the *simultaneous* absorption of two photons) instead of a conventional one-photon excitation offers a number of advantages. These include the ability for a highly confined excitation (and intrinsic three-dimensional resolution) and increased penetration depth by replacing typical one-photon excitation in the UV–visible blue region by two-photon excitation in the visible red–NIR region, owing in particular to the reduction of scattering losses.

Most of these applications strongly benefit from the use of chomophores displaying very high TPA cross-sections in order to significantly decrease the excitation intensity or provide improved excitation efficiency and selectivity. Indeed, in recent years a considerable effort has been devoted to the design and investigation of chromophores with large TPA cross-sections, exploring in particular dipolar[10,15–20] and quadrupolar,[17,21–38] structures. Lately, attention has turned towards multipolar[39–43] and conjugated branched structures[44–51] including dendrimers.[52–55]

Depending on the targeted applications, two-photon chromophores also have to satisfy additional requirements. For instance, the use of such chromophores for biological multiphotonic imaging calls for the design of fluorophores combining a high fluorescence quantum yield (Φ) and TPA cross-section (σ_2) in the spectral range of interest (*i.e.* 700–1200 nm)[56] several orders of magnitude larger than endogenous chromophores (whose TPA cross-sections range between 10^{-5} to about 1 GM).[13] This would open the route for *selective* excitation of two-photon chromophores leading to significantly improved signal to noise ratio (reduction of background fluorescence) and reduction of photodamage.[57] Low (photo)toxicity and high photostability are important additional criteria.

Recently semiconductor nanocrystals (quantum dots: QDs) have been shown to provide a particularly effective approach to fluorescent nano-objects with extremely large

[a] *Synthèse et Electrosynthèse Organiques (CNRS, UMR 6510), Institut de Chimie, Université de Rennes 1, Campus Scientifique de Beaulieu, Bât. 10A, F-35042 Rennes Cedex, France. E-mail: mireille.blanchard-desce@univ-rennes1.fr; Fax: + 33 2 23 23 62 77*
[b] *Laboratoire de Chimie de Coordination, CNRS, 205 route de Narbonne, F-31077 Toulouse Cedex 4, France. E-mail: majoral@lcc-toulouse.fr; Fax: +33 5 61 55 30 03*
[c] *Dipartimento di Chimica GIAF, Università di Parma, Parco Area delle Scienze 17/A, 43100 Parma, Italy*

† This paper was published as part of the special issue on Dendrimers and Dendritic Polymers: Design, Properties and Applications.

TPA cross-sections ($\sigma_2\Phi$ up to 47 000 GM)[58] overcoming the TPA responses of molecular two-photon fluorophores. QDs have gained tremendous popularity for imaging applications due to their intense, tunable (*e.g.* depending on the size and composition) and robust photoluminescence properties.[59] However, these inorganic systems suffer from several drawbacks such as biological toxicity[60] (due in particular to the presence of heavy metals such as cadmium) and blinking. In addition their surface functionalization for different purposes such as targeting, recognition, conjugation to biomolecules or specific labeling is possible but not undemanding. These inorganic nano-objects also raise a number of questions with respect to environmental issues. The implementation of alternative strategies towards ''soft'' and biocompatible substitutes is thus of high interest. Recently, we have developed a promising route towards all-organic nanodots showing competitive two-photon brightness (comparable to the highest reported for QDs).[61] This route is based on the confinement of a large number of two-photon fluorophores showing significant TPA cross-sections within single spherical nano-objects. Such nanodots can be obtained by grafting two-photon (TP) fluorophores on the surface of a dendrimeric platform (Fig. 1). This modular strategy offers several potential advantages: photoluminescence (PL) characteristics can, in principle, be tuned by playing on the nature of the fluorophore, while the dendrimer scaffold can be chosen so as to minimize toxicity effects and control clearance ability.[62] However, implementing such modular approach also requires taking into account interactions between the various molecular building blocks including possible interactions between decorating fluorophores. The confinement of fluorophores within the nanodot imposes close proximity between chromophores which favors interchromophoric interactions: (i) in the ground state with potential effects on the absorption characteristics and (ii) in the excited state with impending marked effects on PL. Such interactions can significantly affect the optical responses and photophysical properties of the nanodots which will then differ from the mere addition of the contributions of isolated single fluorophores. For instance formation of dimers or aggregates between adjacent fluorophores could lead to fluorescence quenching.[63] Also interactions in the excited state can lead to changes of PL characteristics due to various phenomena (energy transfer, excimer formation or exciton annihilation which is an important decay process in chromophore decorated dendrimers at high excitation intensity[64]).

Also it has been shown that interactions between chromophores within dimers[65] or aggregates[36,66] can lead to significant change in TPA responses. Such effects are expected to be strongly dependent on both the nature of the chromophores and their proximity and relative orientations. In this respect the geometry and symmetry of the dendritic scaffold are expected to play an important role.

In this prospect, we have investigated and compared the photophysical and TPA properties of two series of organic nanodots of different geometries: spherical-like organic nanodots (SOND, Fig. 1) and dumbbell-like organic nanodots (DOND, Fig. 2) built from the gathering of an exponentially increasing number of two-photon active fluorophores **F** on the periphery of dendrimeric platforms of different symmetry. The SOND series is the prototypical organic dots series that was recently prepared as a proof of concept test series.[61] In this work, we examine how the two-photon absorption and PL properties are affected by the nature and symmetry of the dendrimeric scaffold. The SOND series **G1–G4** is derived from a dendritic scaffold built from a C_3 symmetry cyclotriphosphazene core whereas the DOND series **G1′–G′2** is derived from a dendritic scaffold built from an elongated rod-like fluorophore. The different symmetry of the cores induces a difference in both the number and the symmetry of the arrangement of the two-photon fluorophores on the surface of the organic nanodot. In the case of SOND series, the two-photon fluorophores on the surface experience similar environment in relation with the symmetry of the core of the dendrimeric scaffold which controls the overall geometry and topology (Fig. 1). In contrast, the decorating fluorophores of the DOND series clearly experience inhomogeneous environments due to different nature and topology of the core (Fig. 2). This can play a significant role in terms of interchromophoric interactions. If this is the case, the PL characteristics of compounds of the SOND and DOND series can significantly differ for a similar number of decorating fluorophores but a different topology. This is expected to affect the TPEF efficiency of the nanodot. Another important issue with respect to the TPEF efficiency is the variation of the overall TPA cross-

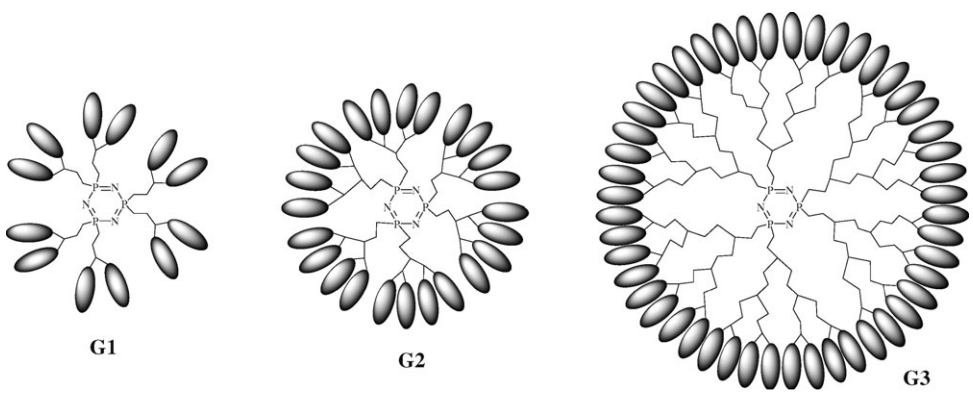

Fig. 1 Schematic representation of homochromophoric spherical-type organic nanodots (SOND).

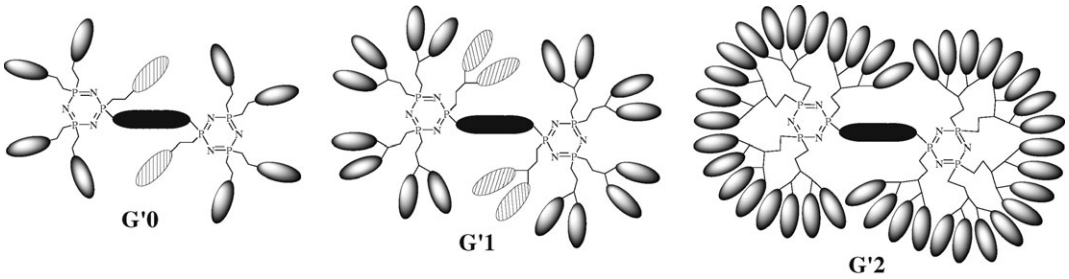

Fig. 2 Schematic representation of heterochromophoric dumbbell-like organic nanodots (DOND).

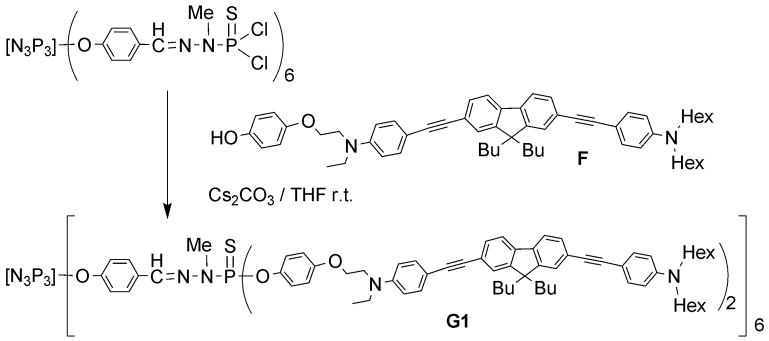

Scheme 1 Synthesis of spherical dendrimer **G1**.

section as a function of the topology. Additive contributions of the two-photon fluorophores to the overall TPA efficiency of the nanodot was observed in the case of the SOND series.[61] Since the environment and the packing of the decorating fluorophores may differ in the two series, modification of their TPA efficiency cannot be excluded. Finally whereas in the case of the SOND series, energy transfer can occur among similar fluorophores on the periphery (excitation energy migration), energy transfer can in principle (depending on the nature and spectroscopic characteristics of the core chromophore) occur both along the surface (homotransfer) and between the core and the surface of the nanodot (heterotransfer) in the DOND case.

Results and discussion

Synthesis

The synthesis of the spherical-like first generation dendrimer **G1** was carried out by grafting 12 equivalents of the TPA chromophore **F** to the $P(S)Cl_2$ end groups of the first generation phosphorus dendrimer[67–69] built from a cyclotriphosphazene core[70] (Scheme 1). The same reaction carried out with the second, third and fourth generations of the same series of dendrimers afforded the spherical dendrimers **G2**, **G3** and **G4**, respectively (Fig. 3), as previously reported.[61]

Two series of dumbbell-like dendrimeric compounds were synthesized, both issued from the same biphenolic chromophore **2**[71] (Scheme 2) as the starting compound. The first series (**C0**, **C1**) was synthesized to serve as model for the photophysical properties of the core fluorophores of the other series (*i.e.* DOND series). The synthesis of the generation 0 of the monochromophoric series **C0** necessitates first the isolation of the pentasubstituted cyclotriphosphazene **1**, which is then reacted with chromophore **2**. The substitution of the sixth Cl of the cyclotriphosphazene with such bulky substituent is slow and needs 7 days to go to completion (Scheme 2). ^{31}P NMR is particularly suitable to monitor this reaction; indeed the

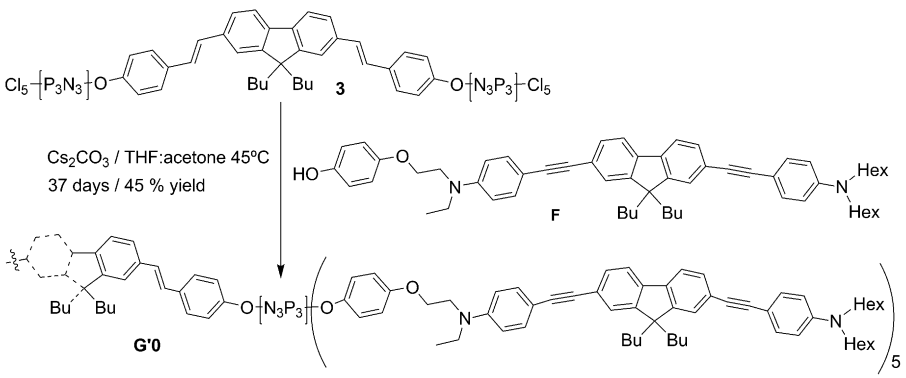

Fig. 3 Structures of spherical-type dendrimers **G2–G4**.

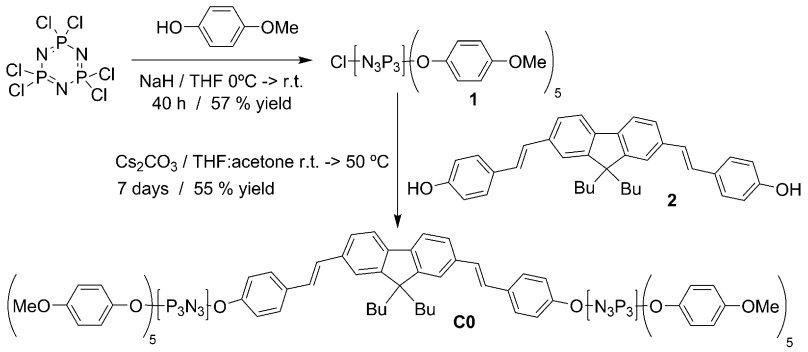

Scheme 2 Synthesis of monochromophoric model **C0**.

spectrum of compound **1** displays an ABB′ system, whereas the sixth substitution induces an AA′A″ system for **C0**, affording a narrow multiplet.

The generation 0 of the multichromophoric series of dumbbell-like dendrimers (*i.e.* DOND series) is synthesized using a different route. Indeed, in this case $N_3P_3Cl_6$ (large excess) is reacted with the biphenol **2** to afford compound **3**.[71] In the second step, 10 equivalents of the two-photon fluorophore **F**[61] are grafted to afford after a prolonged heating (37 days) the generation 0 of the dumbbell-like multichromophoric dendrimer **G′0** (Scheme 3). In this case also, ^{31}P NMR is an invaluable tool, since the completion of the reactions is shown by the appearance of a narrow multiplet, observed after a series of intermediate compounds displaying ABB′ type spectra.

First generation compounds of both monochromophoric and multichromophoric dumbbell-like dendrimers are synthesized by grafting phenols to the $P(S)Cl_2$ end groups of dendrimer **4**.[71] The monochromophoric model compound **C1** is obtained by reaction with HO–C_6H_4–OMe, whereas the multichromophoric compound **G′1** is obtained by reaction with fluorophore **F** (Scheme 4, Fig. 2). In both cases, the narrow multiplet (due to the unsymmetrical substitution on the N_3P_3 groups) observed at 62.4 ppm for the $P(S)Cl_2$ end groups by ^{31}P NMR is replaced by another narrow multiplet at 64.5 ppm. An intermediate signal observed at 69.4 ppm and corresponding to the monosubstitution (P(S)ClOAr) totally disappears when the reaction is over. The same method is applied for the synthesis of the second generation of the dumbbell-like multichromophoric dendrimer **G′2**. This compound possesses two types of chromophoric units: one at the core and 40 as end groups (Scheme 5, Fig. 2).

Photophysical properties

One-photon absorption. All dendrimers show a strong absorption band in the near UV–visible-blue region (Table 1). The normalized absorption spectra of the multichromophoric dendrimers of the SOND series overlap almost perfectly with the absorption spectrum of the isolated decorating fluorophore **F** with only a slight broadening at the red tail (Fig. 4). The molar extinction coefficients increase almost linearly with the number of decorating fluorophores leading to giant absorption coefficients for the **G4** SOND dendrimer (Table 1).[72] These trends suggest that no noticeable interactions occur in the ground state.

The absorption spectra of dendrimers of the dumbbell-like series (DOND dendrimers) are broader and slightly blue-shifted with respect to that of the SOND dendrimers (Table 1, Fig. 4). The absorption spectra of the core chromophores (**C0** for **G′0** and **C1** for **G′1** and **G′2**) mostly overlap, have comparable extinction coefficient and are only slightly blue-shifted with respect to that of peripheral fluorophores **F** (Table 1, Fig. 5). However, comparison of the absorption spectra of dendrimers of the DOND series with that corresponding to that expected for an *additive* contributions of core and peripheral chromophores **F** (Fig. 6) shows that the assembly of two-photon fluorophores **F** in the DOND series leads to broader spectra and lower effective absorption coefficient per fluorophore. This indicates a larger inhomogeneous

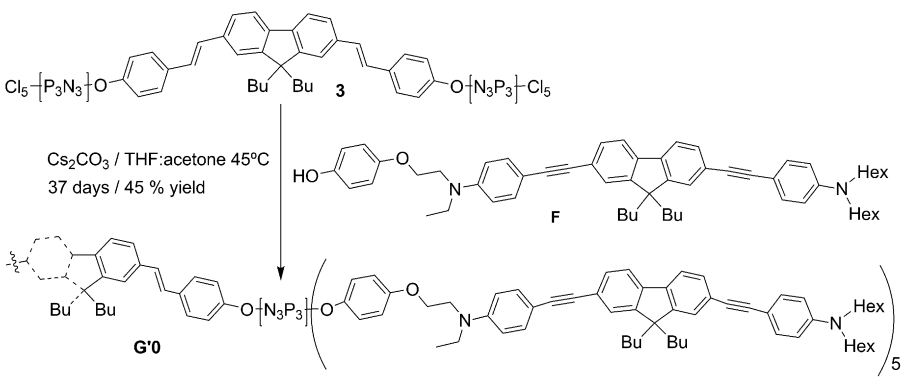

Scheme 3 Synthesis of dumbbell-like multichromophoric compound **G′0** (only half of the molecule is represented for **G′0**).

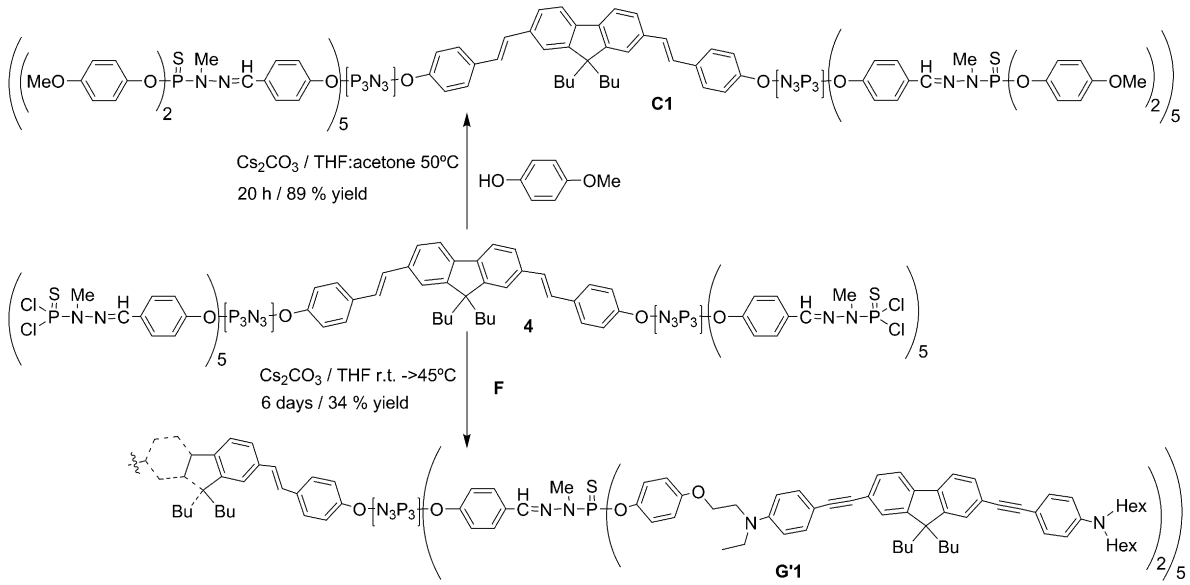

Scheme 4 Synthesis of monochromophoric dendrimer **C1** and dumbbell-like dendrimer **G′1** (only half of the molecule is represented for **G′1**).

broadening suggesting that the decorating fluorophores of the DOND series experience a larger range of environments (and disorder) in relation with the different geometry and lower symmetry of their arrangement within the nanodots.

Fluorescence. The emission spectra of dendrimers of the SOND series clearly show a change of the emission band shape and position with increasing generation number (Fig. 4). A change of the vibronic relative intensities is observed along with a red-shift of the emission maxima (Table 1). Whereas the 0–0 transition is clearly the more intense vibronic band in the emission spectrum of the parent isolated fluorophore **F**, the 0–1 transition becomes more intense in the dendrimers and this effect becomes stronger on going from **G1** to **G2** compounds (Fig. 4). The change in vibronic structure reveals an increase in reorganization energy in the dendrimers as compared to the isolated fluorophore, indicating that the emitting fluorophore has stronger interactions with its environment when gathered on the surface of the dendrimer. Indeed the proximity of adjacent chromophores modifies the local environment of the emitting fluorophore as compared to an isolated fluorophore surrounded only by solvent molecules. The loss of fine vibronic structure, red-shift and spectral broadening of the emission band with increasing generation number suggests that the polarity of the environment of the emitting fluorophores is increasing. It should be stressed that the emission of quadrupolar chromophore **F** is very sensitive to polarity[73] allowing its use as a probe of its local environment. Fig. 7 shows emission spectra calculated by the aid of the model reported in ref. 73, for different environmental reorganization energies (ε_{or}). Parameters used are the same as reported in ref. 73, since the chromophore is the same. In the adopted model, the evolution of position and shape (together with inhomogeneous broadening effects) of the emission band of some quadrupolar chromophores (belonging to class **I** as defined in ref. 73), is ascribed to symmetry breaking in the relaxed excited state. Polar environments stabilize broken-symmetry states, corresponding to dipolar states. The dipolar nature of the broken-symmetry relaxed excited state is thus responsible for the solvatochromic behavior of fluorescence bands. In

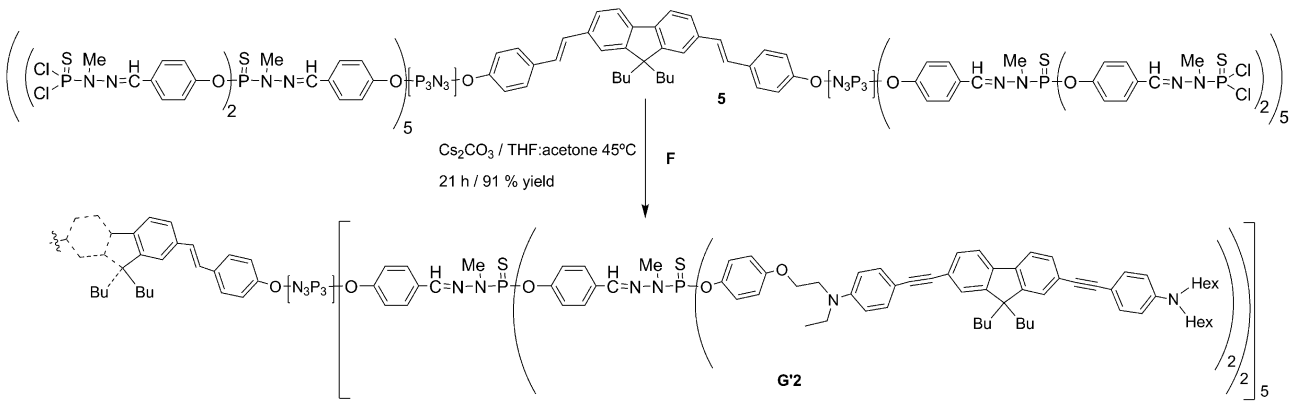

Scheme 5 Synthesis of dumbbell-like dendrimer **G′2** (only half of the molecule is represented for **G′2**).

Table 1 Photophysical data for fluorophore **F** and dendrimers **G1–G4** (SOND), **C0–C1** (model dumbbell-like chromophores) and **G′0–G′2** (DOND) in toluene

	No. of fluorophores	MW/g mol^{-1}	λ_{abs}/nm	ε/M^{-1} cm^{-1}	λ_{em}/nm	Φ^a	τ/ns^b	r^c	σ_2 (max.)^d/GM
F	1 **F**	841	386	84 900	420	0.83	0.67	0.18	765
G1	12 **F**	11 485	385	1 004 000	423	0.75	0.71	0.03	8880
G2	24 **F**	24 102	386	2 035 000	426	0.71	0.69	0.02	17 700
G3	48 **F**	49 335	386	3 785 000	441	0.62	0.71	0.01	29 800
G4	96 **F**	99 804	386	7 101 000	445	0.48	0.66	0.01	55 900
C0	1 **C0**	2014	377	73 100	410	0.81	0.82	0.22	124
C1	1 **C1**	5377	378	71 500	412	0.68	0.85	0.28	146
G′0	1 **C0** + 10 **F**	9184	382	805 000	443	0.44^e	0.88^f	—^{g}	7100
G′1	1 **C1** + 20 **F**	19 698	382	1 537 000	444	0.11^e	0.71^f	—^{g}	14 300
G′2	1 **C1** + 40 **F**	40 726	384	3 000 000	445	0.26^e	0.65^f	—^{g}	32 800

^{a} Fluorescence quantum yield determined relative to fluorescein in 0.1 M NaOH. ^{b} Experimental fluorescence lifetime measured by time-correlated single photon counting. ^{c} Steady-state fluorescence anisotropy (λ_{exc} = 382 nm). ^{d} 1 GM = 10^{-50} cm^4 s photon^{-1}. ^{e} Determined for λ_{exc} = λ_{abs}(max.). ^{f} Determined for λ_{em} = λ_{em}(max.). ^{g} Anisotropy is wavelength-dependent (see Fig. 9).

Fig. 7, the variation of ε_{or} nicely describes the evolution of the emission spectrum in different dendrimer generations and symmetries (this correspondence is summarized in the legend). Increasing dendrimer generation corresponds to increased ε_{or} values: chromophores act as dielectrics, more polar than the dissolving solvent (toluene). The effect of solvent polarity and that of dendrimer generation/shape are very similar, on the band position and shape. For example, we can estimate that the polarity of the nanodots varies from lower than that of $CHCl_3$ for low-generation nanodots, up to almost that of acetone for high-generation nanodots.

A distinct feature of the emission characteristics of dendrimers of the SOND series is their low anisotropy values. Parent fluorophore **F** exhibits anisotropy of 0.18 in toluene, whereas

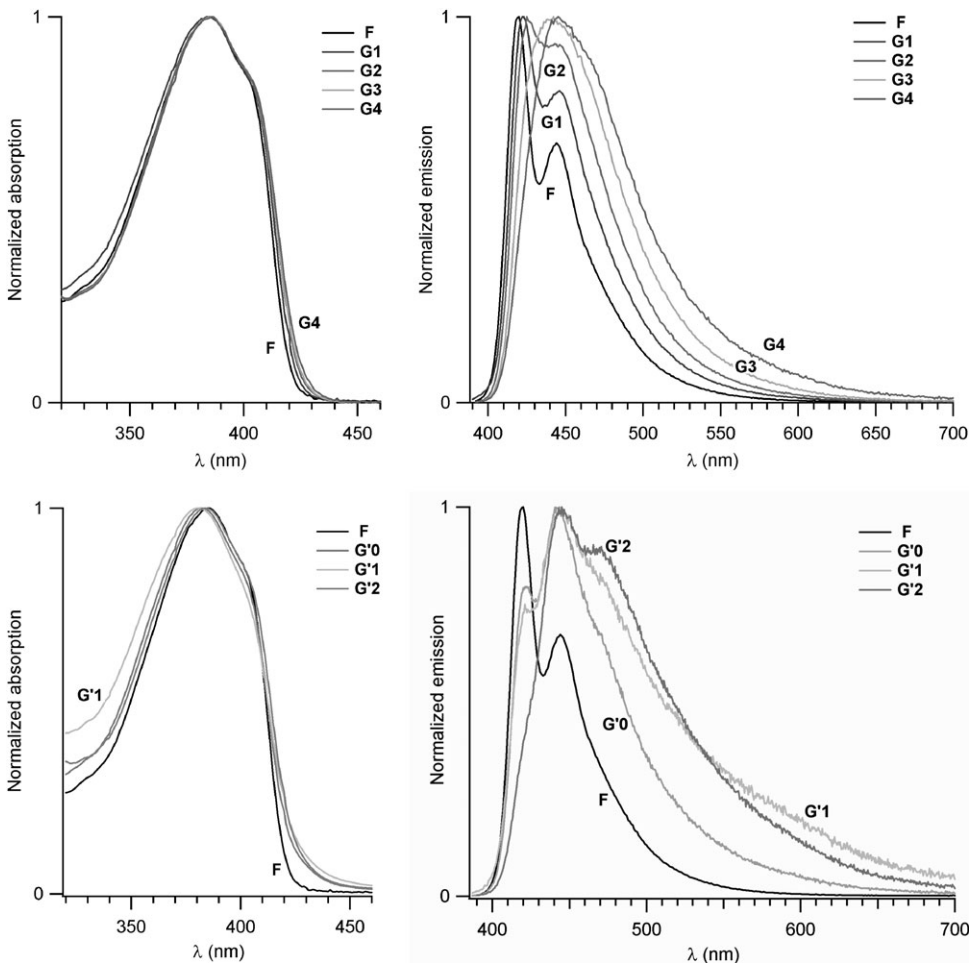

Fig. 4 Normalized absorption and emission spectra (λ_{exc} = λ_{abs}(max.)) in toluene of SOND **G1–G4**, and DOND **G′0–G′2**. The absorption and emission spectra of fluorophore **F** in toluene are also included for evaluation of the effect of the gathering of fluorophores **F** on the surface of dendritic nanodots.

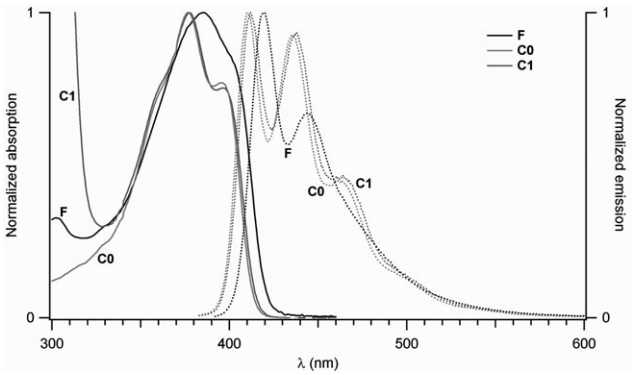

Fig. 5 Normalized absorption and emission spectra ($\lambda_{exc} = \lambda_{abs}$ (max.)) in toluene of model chromophore **F** and model dendrimers **C0–C1**.

G1–G4 display much lower anisotropies, with values ranging between 0.03 and 0.01 (Table 1). Since rotational diffusion of the SOND dendrimers is expected to be much slower than that of **F** due to their size (the radius of dendrimer **G4** is estimated to about 4 nm), the depolarization can be ascribed to fast energy transfer between adjacent decorating fluorophores[74–79] (excitation energy migration or homotransfer).[80] We observe that the fluorescence lifetimes remain roughly unchanged (Table 1) which is consistent with the hypothesis of homochromophoric energy transfer. Indeed homotransfer is possible *via* a Förster mechanism[81] given the non-negligible overlap between absorption and emission spectra of decorating fluorophores. We also observe a continuous decrease of the fluorescence quantum yield with increasing generation number (Table 1). This could be due to the occurrence of traps leading to fluorescence quenching or formation of excimers (consistent with an increasing red-tail) with lower fluorescence quantum yields.[82] The number of traps is expected to statistically increase with increased generation number which could explain the variation of fluorescence quantum yield.

The analysis of the variation of the emission of dendrimers of the DOND series is more intricate because their emission stems from both core and peripheral fluorophores (Fig. 4). The low-energy absorption bands of model core (**C0**, **C1**) and peripheral (**F**) compounds show a major overlap (Fig. 5) and similar intensities (Table 1) making selective one-photon excitation of only one type of chromophore unattainable. In addition, we observe that the emission spectra of model compounds in toluene show a significant overlap, the emission of fluorophore **F** being slightly red-shifted (Fig. 5). Emission spectra of DOND dendrimers **G′0–G′2** show significant differences as compared to their SOND analogues bearing similar number of decorating fluorophores (*i.e.* **G1–G3**). The emission band of DOND dendrimers **G′0–G′2** are clearly red-shifted and broadened (in particular in the red side) with respect to their SOND analogues **G1–G3** (Fig. 8). A possible explanation is that the emitting fluorophores in the DOND dendrimers experience a different environment than in the corresponding SOND dendrimers. This could be attributed to the proximity not only of adjacent identical decorating fluorophores but also of the core chromophore. The decorating fluorophores located close to the core (shown in hashed in Fig. 2) clearly experience different environment. Simulations based on the model reported in ref. 73 also indicate that DONDs are more polar objects than corresponding SONDs (see Fig. 7), suggesting a closer packing of chromophores in DONDs. This finds a possible confirmation in the lower fluorescence quantum yield of DONDs with respect to corresponding (*i.e.* containing approximately the same number of chromophores) SONDs.

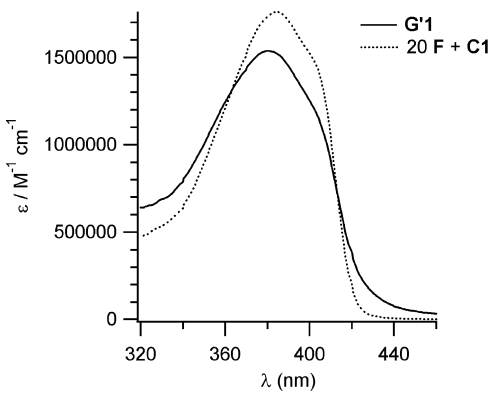

Fig. 6 Comparison of experimental and theoretical (evaluated from additive contributions of isolated constituting chromophores **F** and **C1**) absorption spectra of dendrimer **G′1**.

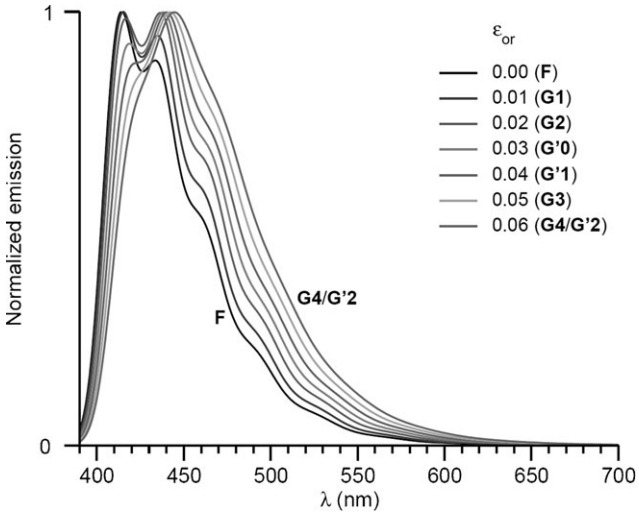

Fig. 7 Emission spectra calculated according to model presented in ref. 73 using parameters relevant to the model chromophore (**F**) for different solvent reorganization energies (see legend, eV units).

In addition, interchromophoric interactions in the excited state (leading to formation of excimer, or hetero-excimer if the core chromophore is involved) can be facilitated in the case of the DOND series due to the larger inhomogeneous broadening and difference (disorder) in packing of the decorating fluorophores on the surface of the DOND dendrimers. Such phenomenon could explain the even more pronounced red tail in the emission band of dendrimers of the DOND series (Fig. 8). Interestingly, the more pronounced red tail is observed for **G′1** which also gives rise to the largest inhomogeneous broadening of the absorption spectra (Fig. 4).

As opposed to the case of homochromophoric dendrimers of the SOND series whose anisotropy values remain constant in the whole emission range (400–600 nm), a continuous

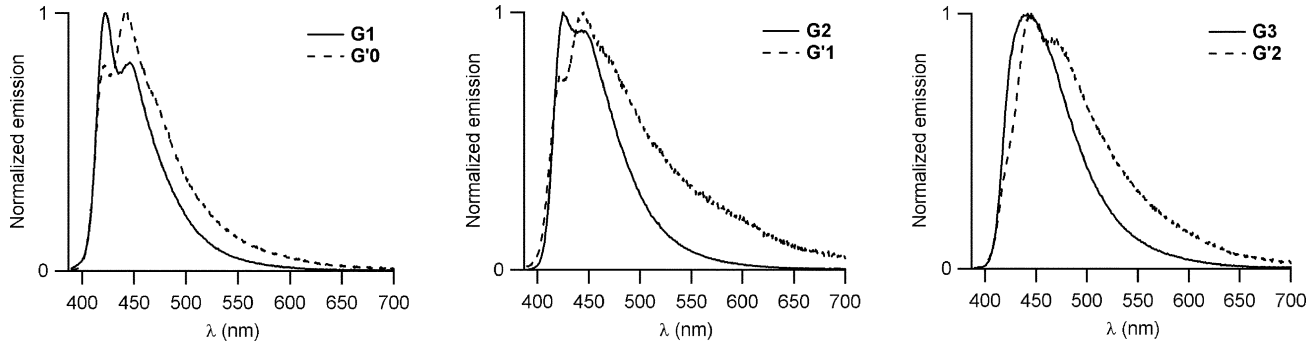

Fig. 8 Comparison of the emission spectra of corresponding spherical-type and dumbbell-like nanodots in toluene.

decrease of the anisotropy value with increasing emission wavelength (from ~0.1 at 400 nm to ~0.02 at 600 nm) is observed in the case of heterochromophoric dendrimers of the DOND series (Fig. 9). This can be attributed to the contribution of two types of fluorophores (namely the core chromophore and the peripheral fluorophores) with different individual anisotropies, the combination of which results in a wavelength-dependent global anisotropy. Whatever the wavelength, the anisotropy values are lower than that of their constituting chromophoric units (see *r* values for **F** and **C0** or **C1** in Table 1).[83] These low values for such large nano-objects indicate that fast energy transfer also takes place in the DONDs. For wavelengths higher than 550 nm, where emission stems only from the peripheral chromophores (see Fig. 4 and 5), the anisotropy values are similar to that of homochromophoric SONDs indicative of fast energy transfer involving the peripheral chromophores. The larger values obtained at lower wavelength can be related to the increasing contribution of the core chromophore, whose emission is blue-shifted with respect to that of peripheral fluorophores (Fig. 6).[84]

Another important feature is the much lower fluorescence quantum yield of the dendrimers of the DOND series as compared to those of the SOND series (Table 1).[85] This could be related to interactions between chromophores giving rise to competing processes such as fast energy transfer between adjacent chromophores and formation of (red-shifted) excimers or hetero-excimer with lower fluorescence quantum yield. This is consistent with the rise of a red tail in the emission band which is even broader than in the case of the SOND dendrimers (Fig. 8). Strikingly dendrimer **G′1** which is the less fluorescent of the DOND series shows the more pronounced red tail. Also, the larger disorder (as testified by the inhomogeneous broadening) within decorating fluorophores—due to the different geometry of the dendrimers of the DOND series as compared to the SOND series-can be responsible for different overlap and interactions between the chromophores on the periphery.

Two-photon absorption

The TPA of the dendrimers was studied by investigating the TPEF of SOND and DOND dendrimers in toluene. TPEF measurements allow for direct measurement of the TPEF action cross-section $\sigma_2\Phi$, the relevant figure of merit for imaging applications.

The TPA spectra of dendrimers **C0** and **C1** were determined as reference for the TPA response of core chromophores in the DOND series. These model chromophores clearly show much lower TPA cross-section than decorating fluorophore **F** over the whole spectral range (Fig. 10) and their maximum TPA cross-sections are more than five times smaller (Table 1). As a

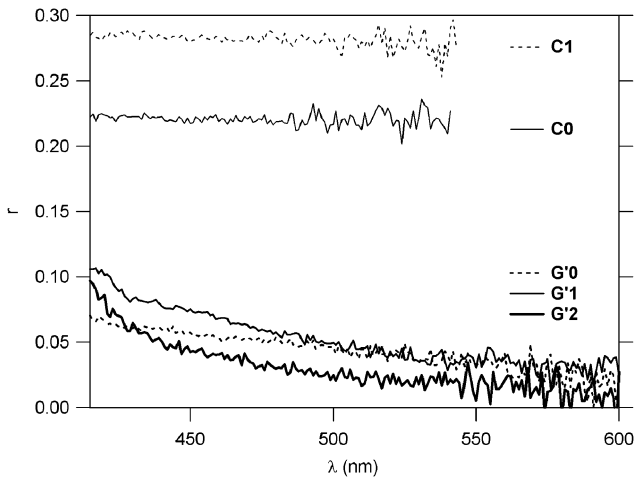

Fig. 9 Emission anisotropy of monochromophoric dendrimers **C0–C1** and dumbbell-like nanodots **G′0–G′2** in toluene (λ_{exc} = 382 nm).

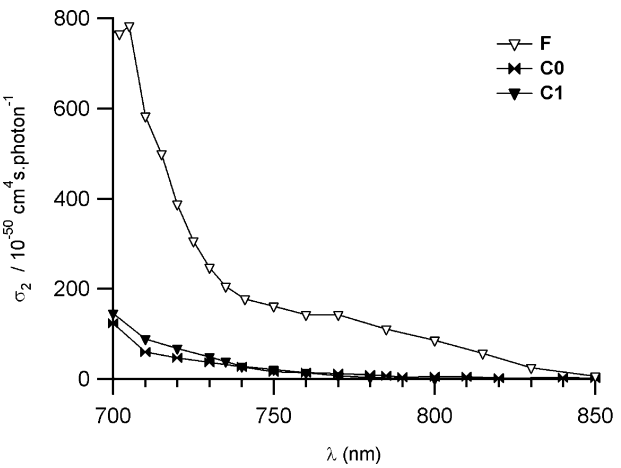

Fig. 10 Two-photon absorption spectra of model fluorophore **F** and monochromophoric dendrimers **C0–C1** determined by femtosecond TPEF measurements in toluene.

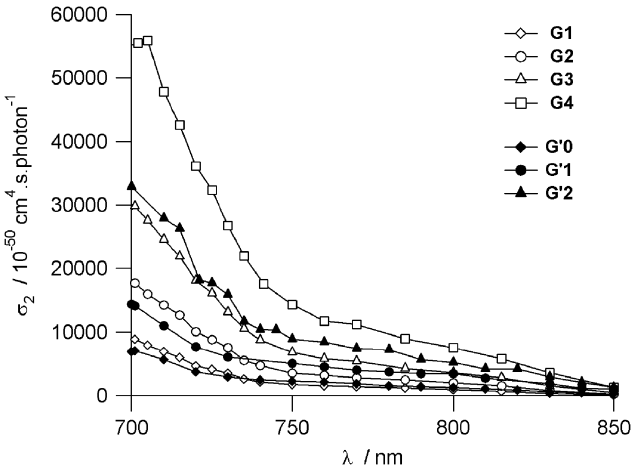

Fig. 11 Two-photon absorption spectra of SOND (**G1–G4**) and DOND (**G′0–G′2**) dendrimers determined by femtosecond TPEF measurements in toluene.

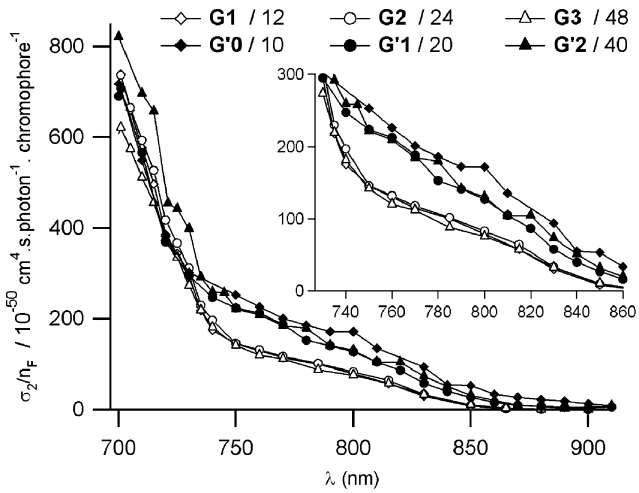

Fig. 12 Comparison of the TPA efficiency (normalized by the number of TP fluorophores per nanodot) of SOND and DOND. Inset: zoom of the 720–860 nm region (in the same units).

result, the TPA response of dendrimers of the DOND series is expected to be dominated by the contribution of decorating fluorophores given their larger molecular TPA response and large excess (with a **F**/**C** ratio of, respectively 10/1, 20/1 and 40/1 for **G′0**, **G′1** and **G′2**). In addition the TPA response of reference compounds **C0** and **C1** over 750 nm is clearly negligible with respect to that of fluorophore **F**. Hence although selective one-photon excitation of decorating fluorophores of the DOND series was not permitted (similar absorption coefficient and almost complete overlap of the low energy-absorption bands), *selective* two-photon excitation of the decorating fluorophores of heterochromophoric DOND dendrimers becomes possible. This is a major advantage of TP excitation.

The TPA spectra of dendrimers of the SOND and DOND series are shown in Fig. 11. The TPA cross-section in each series of dendrimers increases almost linearly with the number of decorating fluorophores leading to giant TPA cross-sections. This is apparent from the quasi overlap of the TPA spectra normalized by the number of decorating chromophores in the 700–740 nm region (Fig. 12).[86] We observe however a noticeable difference in the TPA spectra of dendrimers of the SOND[87] and DOND series at wavelengths higher than 740 nm. In that spectral range, dendrimers of the DOND series show definitely higher TPA cross-sections than dendrimers of the SOND series. For example at 760 nm, dendrimers of the DOND series show a TPA cross-section normalized by the number of chromophores which is 60% larger than dendrimers of the SOND series. This indicates that the decorating fluorophores (or at least some of them) of the DOND dendrimers show a definitely larger TPA cross-section in the 750–850 nm region. This difference between DOND and SOND nanostructures can be directly related to their different topology and thus to the presence of the core chromophore. Hence although the core chomophores (**C0** or **C1**) show much smaller TPA activity than decorating fluorophores (Fig. 10), their presence affects the TPA response of peripheral fluorophores. This can possibly be attributed to a change of arrangement (relative orientation, packing) of decorating fluorophores due to the different topology of the dendritic architecture or to direct interactions between the core and decorating fluorophores located close to it. Hence, the present study demonstrates that the different topology of the dendrimers of the SOND and DOND series modifies both the PL and TPA properties of the organic nanodots, providing evidence that arrangement and/or environment of the two-photon fluorophores in the organic nanodots can significantly affect their response.

Conclusion

The present study demonstrates that the topology and nature of the dendritic platform considerably influences the PL and TPA properties of the organic nanodots. For comparable numbers of decorating two-photon fluorophores, the PL efficiency of the DOND dendrimers is much poorer due most probably to interactions between the core chromophore and proximal excited fluorophores (combined with fast energy transfer which allows excitation energy migration towards those traps). In contrast, the TPA efficiency is increased for the DOND dendrimers as compared to the SOND dendrimers in a large portion of the investigated spectral range (740–900 nm). Such phenomenon may have different causes. It might be related to the change in topology caused by the different geometry of the core, thus resulting in a different packing and self-orientation of the decorating two-photon fluorophores on the surface of the nanodots. Such effect can indeed lead to changes of the TPA response of decorating fluorophores as compared to isolated ones.[66] Alternatively, the change in TPA response could be due to a direct interaction of the core with its proximal decorating fluorophores. Replacing the chromophoric core by a non-conjugated core having the same shape would allow to discriminate these causes. In any case, this raises an important question since the global TPA efficiency is found to be different for the two series. This opens an interesting route towards improved TPA efficiency of

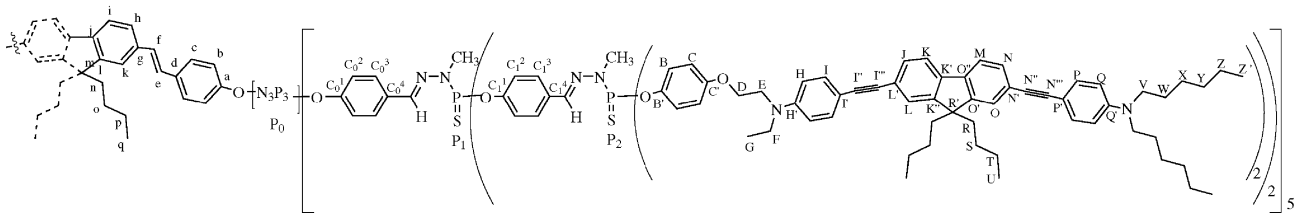

Fig. 13 Numbering used for NMR assignments (only half of the molecule is represented).

the nanodots by controlling the relative orientation of the decorating fluorophores and or their environment.

We have also demonstrated in this study that all-organic nanodots can exhibit two-photon absorption and two-photon brightness comparable to the highest values reported for quantum dots[58] and represent thus a promising complementary approach towards fluorescent labels for TPEF imaging applications. The highly modular design of nanodots allows adjunction of supplementary layers, decoration of the periphery with hydrosolubilizing groups, and insertion of functional groups that could be utilized for bioconjugation purposes. In that way, we have very recently reported[71] biocompatible water-soluble monochromophoric nanodots with shielding dendrimeric layers and peripheral ammonium groups, that maintain their quantum efficiency in water and in physiological environment, and the efficiency of which as contrast agents has been demonstrated for *in vivo* TPEF imaging on living animal.

Experimental

General

All manipulations were carried out with standard high vacuum and dry-argon techniques. The solvents were freshly dried and distilled (THF and ether over sodium/benzophenone, pentane and CH_2Cl_2 over phosphorus pentoxide). Reactions were monitored by thin layer chromatography on Merck silica gel 60 F254 precoated aluminum sheets. Column chromatography: SDS silica gel Si 60 A CC (70–200 μm, 230–400 mesh) or Florisil® (60–100 mesh). Classical ^{1}H, ^{13}C, ^{31}P NMR spectra were recorded with Bruker AC 200, AC 250, or Avance 300, 500 spectrometers. References for NMR chemical shifts are 85% H_3PO_4 for ^{31}P NMR, $SiMe_4$ for ^{1}H and ^{13}C NMR. The attribution of ^{13}C NMR signals has been done using J_{mod}, two dimensional HMBC, and HMQC, Broad Band or CW ^{31}P decoupling experiments when necessary. The multiplicity of ^{13}C NMR signals is indicated only when the signal is not a singlet. The numbering used for the assignment of NMR signals is shown in Fig. 13.

Syntheses

Compound 1. Sodium hydride (0.18 g, 7.04 mmol) and dry THF (20 mL) were introduced into a 50 mL Schlenk. 4-Hydroxyanisole (0.74 g, 5.91 mmol) was added to this suspension. Once the solution was clear, it was cooled to 0 °C in a water–ice bath and hexachlorocyclotriphosphazene (0.40 g, 1.14 mmol) was added at once. The reaction was stirred while allowing the temperature to rise slowly to room temperature. The reaction was considered to be finished after 40 h (^{31}P NMR monitoring), then the salts were centrifuged, and the solvent was removed. The pentasubstituted core was separated from the tetra- and hexasubstituted analogues by column chromatography on silica gel using mixtures of hexanes and ethyl acetate of increasing polarity (9.1 to 8.2). The pure product (0.50 g, 57% yield) was obtained as a colorless oil.

^{1}H NMR ($CDCl_3$, 300.1 MHz), δ (ppm) = 3.78 (s, 15H, OCH_3), 6.72 (d, J = 9.0 Hz, 2H, C_0^{3A}–H), 6.73 (d, J = 9.0 Hz, 4H, C_0^{3B}–H), 6.79 (d, J = 9.0 Hz, 4H, C_0^{3B}–H), 6.87 (dd, J = 9.0 Hz/J = 1.8 Hz, 2H, C_0^{2A}–H), 6.92 (d, J = 9.0 Hz, 4H, C_0^{2B}–H), 7.06 (d, J = 9.0 Hz, 4H, C_0^{2B}–H). ^{31}P{^{1}H} NMR ($CDCl_3$, 121.5 MHz), δ (ppm) = 8.07 (d, J = 81.5 Hz, P_0^B), 8.08 (d, J = 78.0 Hz, P_0^B), 23.10 (dd, J = 78.0 Hz/J = 81.5 Hz, P_0^A). ^{13}C NMR ($CDCl_3$, 75.5 MHz), δ (ppm) = 157.04 (d, J = 2.26 Hz, C_0^{4A}), 156.87 (C_0^{4B}), 156.74 (C_0^{4B}), 144.01 (pseudo t, J = 3.81 Hz, C_0^{1B}), 143.85 (pseudo t, J = 3.81 Hz, C_0^{1B}), 143.75 (pseudo d, J = 9.81 Hz, C_0^{1A}), 122.15 (pseudo t, J = 2.26 Hz, C_0^{2B}), 122.09 (m, C_0^{2A}), 121.84 (pseudo t, J = 2.26 Hz, C_0^{2B}), 114.39 (C_0^3), 55.53 (OCH_3), 55.51 (OCH_3).

Model compound C0. The pentasubstituted cyclotriphosphazene **1** (0.11 g, 0.14 mmol) and dry THF (2.5 mL) were introduced into a 50-mL Schlenk. The biphenolic chromophore **2**[71] (0.036 g, 0.07 mmol) and caesium carbonate (0.05 g, 0.14 mmol) were added to this solution, and the resulting mixture was stirred at room temperature for two days, then five more days at 50 °C (^{31}P NMR monitoring). The salts were centrifuged off and the solvent was removed by vacuum evaporation. The pure product (0.10 g, 55% yield) was obtained after a column chromatography on silica gel using mixtures of hexane–ethyl acetate of increasing polarity as eluent (9 : 1 → 8 : 2 → 7 : 3 → 5 : 5).

^{1}H NMR ($CDCl_3$, 300.1 MHz), δ (ppm) = 0.63–0.75 (m, 10H, H_q, H_o), 1.14 (m, 4H, H_p), 2.07 (br m, 4H, H_n), 3.76 (s, 12H, CH_3O), 3.80 (s, 18H, CH_3O), 6.69–6.75 (m, 20H, C_0^3–H), 6.84–6.93 (m, 20H, C_0^2–H), 6.98 (d, J = 8.6 Hz, 4H, H_b), 7.16 (m, 4H, H_e, H_f), 7.37 (d, J = 8.6 Hz, 4H, H_c), 7.50 (s, 2H, H_k), 7.53 (d, J = 8.6 Hz, 2H, H_h), 7.71 (d, J = 7.8 Hz, 2H, H_i). ^{31}P{^{1}H} NMR ($CDCl_3$, 121.5 MHz), δ (ppm) = 9.86 (m, P_0). ^{13}C{^{1}H} NMR ($CDCl_3$, 62.9 MHz), δ (ppm) = 13.89 (C_q), 23.14 (C_p), 26.03 (C_o), 40.44 (C_n), 54.97 (C_m), 55.53 (OCH_3), 114.34 (C_0^3), 120.01 (C_i), 120.67 (C_k), 121.34 (m, C_b), 121.92 (m, C_0^2), 125.66 (C_h), 127.02 (C_e), 127.33 (C_c), 129.16 (C_f), 134.22 (C_g), 136.24 (C_d), 140.71 (C_j), 144.30 (m, C_0^1), 150.07 (m, C_a), 151.60 (C_l), 156.56 (C_0^4).

Model compound C1. The first generation dendrimer **4**[71] with the chromophore immobilized in the core (0.038 g, 10.68 μmol), 4-hydroxyanisole (0.030 g, 240.04 μmol), caesium

carbonate (0.150 g, 457.00 μmol), and an acetone–THF (1 : 1) mixture (8 mL) were introduced in a 50-mL Schlenk. The resulting heterogeneous solution was stirred at 50 °C for 20 h. The salts were filtered and the solvent removed when the reaction was finished (^{31}P NMR monitoring). The crude product was dissolved in minimum amount of chloroform and added dropwise to 300 mL of pentane under vigorous stirring, and the precipitated product recovered by filtration (for three times) to afford the pure chromophoric core model **C1** (0.051 g, 89% yield).

^{1}H NMR ($CDCl_3$, 300.1 MHz), δ (ppm) = 0.53–0.69 (m, 10H, H_q, H_o), 1.09 (m, 4H, H_p), 2.02 (br m, 4H, H_n), 3.25 (d, $^{3}J_{H-P}$ = 10.2 Hz, 30H, CH_3N), 3.70 (s, 20H, CH_3O), 3.72 (s, 10H, CH_3O), 3.73 (s, 30H, CH_3O), 6.78 (d, J = 9.0 Hz, 40H, C_1^3–H), 6.99–7.16 (m, 68H H_c, H_e, H_f, C_0^2–H, C_1^2–H), 7.36–7.44 (m, 8H, H_h, H_k, H_b), 7.56–7-66 (m, 32H, H_i, C_0^3–H, CH═N). ^{31}P{^{1}H} NMR ($CDCl_3$, 121.5 MHz), δ (ppm) = 8.47 (m, P_0), 64.30 (s, P_1), 64.40 (s, P_1). ^{13}C{^{1}H} NMR ($CDCl_3$, 62.9 MHz), δ (ppm) = 13.91 (C_q), 23.08 (C_p), 26.00 (C_o), 33.11 (d, J_{C-P} = 12.1 Hz, CH_3N), 40.69 (C_n), 55.00 (C_m), 55.52 (OCH_3), 114.49 (C_1^3), 120.06 (C_i), 120.67 (C_k), 121.12 (m, C_b), 121.41 (m, C_0^2), 122.28 (d, J_{C-P1} = 4.4 Hz, C_1^2), 125.54 (C_h), 126.73 (C_e), 127.50 (C_c), 129.41 (C_0^3), 129.41 (C_f), 132.24 (m, C_0^4), 134.72 (C_g), 136.02 (C_d), 138.28 (d, J_{C-P1} = 13.8 Hz, C_0H═N), 140.72 (C_j), 144.14 (d, J_{C-P1} = 6.92 Hz, C_1^1), 149.57 (m, C_a), 151.24 (m, C_0^1), 151.56 (C_l), 156.98 (C_1^4).

Dendrimer G′0. The zeroth generation dendrimer **3**[71] (0.005 g, 4.40 μmol), the terminal chromophore **F**[61] (0.039 g, 46.34 μmol), caesium carbonate (0.029, 89.03 μmol), and a 1 : 1 tetrahydrofuran–acetone mixture (6 mL) were introduced in a 50 mL Schlenk, and stirred at 45 °C for 20 days, then for 17 days at 60 °C. The salts were filtered off and the solvent was removed when the reaction was finished (^{31}P NMR monitoring). The product was purified by washing the orange solid with a 1 : 1 acetone–methanol mixture to afford the orange bichromophoric product (0.0182 g, 45% yield).

^{1}H NMR ($CDCl_3$, 500.3 MHz), δ (ppm) = 0.60–0.64 (m, 44H, H_S, H_o), 0.65–0.70 (m, 66H, H_U, H_q), 0.94 (br s, 60H, $H_{Z'}$), 1.10 (m, 44H, H_T, H_p), 1.22 (m, 30H, H_G), 1.36 (m, 120H, H_X, H_Y, H_Z), 1.62 (m, 40H, H_W), 1.99 (m, 44H, H_R, H_n), 3.31 (br s, 40H, H_V), 3.42–3.57 (m, 20H, H_F), 3.63–3.79 (m, 20H, H_E), 3.97–4.14 (m, 20H, H_D), 6.61 (d, J = 7.6 Hz, 20H, H_Q), 6.65 (m, 20H, H_H), 6.70 (d, J = 7.4 Hz, 20H, H_C), 6.91 (m, 20H, H_B), 7.00 (m, 4H, H_b), 7.17 (m, 4H, H_e, H_f), 7.44 (m, 44H, H_I, H_P, H_c), 7.46–7.52 (m, 44H, H_J, H_L, H_N, H_O, H_h, H_k), 7.63 (m, 22H, H_K, H_M, H_i). ^{31}P{^{1}H} NMR ($CDCl_3$, 121.5 MHz), δ (ppm) = 9.68 (m, P_0). ^{13}C{^{1}H} NMR ($CDCl_3$, 125.8 MHz), δ (ppm) = 12.28 (C_G), 13.88 (C_U, C_q), 14.08 ($C_{Z'}$), 22.71 (C_Z), 23.12 (C_T, C_p), 25.89 (C_S, C_o), 26.84 (C_X), 27.23 (C_W), 31.74 (C_Y), 40.25 (C_n), 40.34 (C_R), 45.63 (C_F), 49.59 (C_E), 50.98 (C_V), 55.06 ($C_{R'}$, C_m), 65.82 (C_D), 88.22 ($C_{N''}$), 88.61 ($C_{I''}$), 90.78 ($C_{I'}$), 91.22 ($C_{N'''}$), 108.76 ($C_{P'}$), 110.07 ($C_{I'}$), 111.23 (C_Q), 111.46 (C_H), 114.97 (C_C), 119.73 (C_K, C_M), 120.09 (C_i), 120.71 (C_k), 121.24 (m, C_b), 121.97 (m, C_B), 122.51 ($C_{O''}$), 122.80 ($C_{K'}$), 125.54 (C_L, C_O, C_h), 126.89 (C_e), 127.38 (C_c), 129.17 (C_f), 130.37 (C_J, C_N), 132.89 (C_P), 133.03 (C_I), 134.31 (C_g), 136.12 (C_d), 136.12 (C_d), 140.00 ($C_{N'}$), 140.22 ($C_{L'}$), 140.72 (C_j), 144.56 (m, $C_{B'}$), 147.37 ($C_{H'}$), 147.94 ($C_{Q'}$), 150.12 (m, C_a), 150.93 ($C_{K''}$, $C_{O'}$), 151.71 (C_l), 155.65 ($C_{C'}$).

Dendrimer G′1. The first generation dendrimer **4**[71] (0.010 g, 2.83 μmol), the terminal chromophore **F**[61] (0.049 g, 58.2 μmol), caesium carbonate (0.038, 113.94 μmol) and tetrahydrofuran (7 mL) were introduced in a 50 mL Schlenk, and stirred at room temperature overnight then for 6 days at 45 °C. The salts were filtered off and the solvent removed when the reaction was finished (^{31}P NMR monitoring). The product was purified by column chromatography (Florisil®, $CHCl_3$ to THF–CH_3OH as eluent mixtures) and further diethyl ether washings to afford the orange bichromophoric product (0.0191 g, 34% yield).

^{1}H NMR ($CDCl_3$, 500.3 MHz), δ (ppm) = 0.57–0.63 (m, 84H, H_S, H_o), 0.63–0.70 (m, 126H, H_U, H_q), 0.86–0.96 (m, 120H, $H_{Z'}$), 1.04–1.12 (m, 84H, H_T, H_p), 1.12–1.23 (m, 60H, H_G), 1.30–1.39 (m, 240H, H_X, H_Y, H_Z), 1.52–1.67 (m, 80H, H_W), 1.91–2.06 (m, 84H, H_R, H_n), 3.18–3.30 (m, 30H, P_1–N–CH_3), 3.27–3.36 (m, 80H, H_V), 3.37–3.49 (m, 40H, H_F), 3.60–3.74 (m, 40H, H_E), 3.92–4.06 (m, 40H, H_D), 6.53–6.69 (m, 80H, H_H, H_Q), 6.69–6.83 (m, 40H, H_C), 7.02–7.16 (m, 68H, H_B, C_0^2–H, H_b, H_e, H_f), 7.37–7.44 (m, 84H, H_I, H_P, H_c), 7.44–7.51 (m, 84H, H_J, H_L, H_N, H_O, H_h, H_k), 7.48–7.53 (m, 30H, C_0^3–H, CH═N), 7.58–7.69 (m, 42H, H_K, H_M, H_i). ^{31}P{^{1}H} NMR ($CDCl_3$, 202.5 MHz), δ (ppm) = 8.58 (m, P_0), 64.58 (m, P_1). ^{13}C{^{1}H} NMR ($CDCl_3$, 125.8 MHz), δ (ppm) = 12.22 (C_G), 13.86 (C_U, C_q), 14.05 ($C_{Z'}$), 22.68 (C_Z), 23.09 (C_T, C_p), 25.88 (C_S, C_o), 26.80 (C_X), 27.17 (C_W), 31.70 (C_Y), 33.05 (m, P_1–N–CH_3), 40.30 (C_R, C_n), 45.60 (C_F), 49.50 (C_E), 50.99 (C_V), 55.05 ($C_{R'}$, C_m), 65.69 (C_D), 88.54 ($C_{I'''}$, $C_{N''}$), 91.03 ($C_{I''}$, $C_{N'''}$), 108.81 ($C_{P'}$), 109.91 ($C_{I'}$), 111.41 (C_H, C_Q), 115.04 (C_C), 119.72 (C_K, C_M), 121.36 (m, C_0^2, C_b, C_i, C_k), 122.37 (m, C_B), 122.75 ($C_{K'}$, $C_{O''}$), 125.53 (C_L, C_O, C_h), 127.17 (m, C_c, C_e), 128.38 (C_0^3), 129.01 (C_f), 130.37 (C_J, C_N), 132.17 (m, C_0^4), 132.88 (C_P, C_I), 133.81 (C_g), 136.14 (C_d), 140.17 (m, $C_{L'}$, $C_{N'}$, C_0H═N, C_j), 144.27 (m, $C_{B'}$), 147.33 ($C_{H'}$), 147.85 ($C_{Q'}$), 150.93 (m, $C_{K''}$, $C_{O'}$, C_0^1, C_a, C_l), 156.03 ($C_{C'}$).

Dendrimer G′2. The second generation dendrimer **5**[71] (0.078 g, 0.91 μmol), the terminal chromophore **F**[61] (0.031 g, 36.48 μmol), caesium carbonate (0.026 g, 78.09 μmol) and a 1 : 1 acetone–THF mixture (6 mL) were introduced in a 50-mL Schlenk, and stirred at 50 °C for 21 h. The salts were filtered and the solvent removed when the reaction was finished (^{31}P NMR monitoring). The orange solid obtained was repeatedly washed with diethyl ether until no **F** chromophore was observed by TLC. Then the solid was taken in dichloromethane, filtered, and the solvent was removed to afford the orange bichromophoric product (0.034 g, 91% yield).

^{1}H NMR ($CDCl_3$, 500.3 MHz), δ (ppm) = 0.50–0.74 (m, 410H, H_S, H_U, H_o, H_q), 0.85–0.96 (m, 240H, $H_{Z'}$), 0.99–1.19 (m, 284H, H_G, H_T, H_p), 1.24–1.29 (m, 480H, H_X, H_Y, H_Z), 1.52–1.67 (m, 160H, H_W), 1.85–2.09 (m, 164H, H_R, H_n), 3.12–3.49 (m, 330H, H_F, H_V, P_1-N-CH_3, P_2-N-CH_3), 3.53–3.72 (m, 80H, H_E), 3.87–4.07 (m, 80H, H_D), 6.52–6.67 (m, 160H, H_H, H_Q), 6.68–6.81 (m, 80H, H_C), 7.00–7.25 (m, 148H, H_B, C_0^2–H, C_1^2–H, H_b, H_e, H_f), 7.34–7.44 (m, 164H, H_I,

H_P, H_c), 7.44–7.54 (m, 194H, H_J, H_L, H_N, H_O, $C_0H{=}N$, $C_1H{=}N$, H_h, H_k), 7.54–7.72 (m, 142H, H_K, H_M, C_0^3–H, C_1^3–H, H_i). $^{31}P\{^1H\}$ NMR ($CDCl_3$, 121.5 MHz), δ (ppm) = 8.43 (m, P_0), 62.34 (br s, P_1), 64.62 (br s, P_2). $^{13}C\{^1H\}$ NMR ($CDCl_3$, 125.8 MHz), δ (ppm) = 12.24 (C_G), 13.87 (C_U, C_q), 14.07 ($C_{Z'}$), 22.70 (C_Z), 23.09 (C_T, C_p), 25.88 (C_S, C_o), 26.82 (C_X), 27.22 (C_W), 31.72 (C_Y), 33.02 (m, P_1–N–CH_3, P_2–N–CH_3), 40.30 (C_R, C_n), 45.59 (C_F), 49.51 (C_E), 50.96 (C_V), 55.04 ($C_{R'}$, C_m), 65.72 (C_D), 88.22 ($C_{N''}$), 88.54 ($C_{I''}$), 90.87 ($C_{I'}$), 91.23 ($C_{N'''}$), 108.74 ($C_{P'}$), 109.87 ($C_{I'}$), 111.22 (C_Q), 111.40 (C_H), 115.03 (C_C), 119.72 (C_K, C_M), 121.86 (m, C_0^2, C_1^2, C_b, C_i, C_k), 122.42 (m, C_B), 122.78 ($C_{K'}$, $C_{O''}$), 125.51 (C_L, C_O, C_h), 127.11 (C_c, C_e), 128.38 (C_0^3, C_1^3), 129.05 (C_f), 130.36 (C_J, C_N), 131.59 (C_1^4), 132.34 (C_0^4), 132.88 (C_P), 132.98 (C_I), 133.67 (C_g), 136.18 (C_d), 139.98 ($C_{N'}$), 140.17 (m, $C_{L'}$, $CH{=}N$, C_j), 144.25 (m, $C_{B'}$), 147.33 ($C_{H'}$), 147.93 ($C_{Q'}$), 150.92 (m, $C_{K''}$, $C_{O'}$, C_0^1, C_a, C_l), 151.25 (m, C_1^1), 156.01 ($C_{C'}$).

Photophysical studies

Optical absorption and emission spectroscopy. All photophysical measurements have been performed with freshly-prepared solutions in air-equilibrated toluene at room temperature (298 K). UV/Vis absorption spectra were recorded on a Jasco V-570 spectrophotometer. Steady-state and time-resolved fluorescence measurements were performed on dilute solutions (*ca.* 10^{-6} M chromophore concentration, optical density <0.1) contained in standard 1 cm quartz cuvettes using an Edinburgh Instruments (FLS920) spectrometer in photon-counting mode. Emission spectra were obtained, for each compound, under excitation at the wavelength of the absorption maximum. Fluorescence quantum yields were measured according to literature procedures using fluorescein in 0.1 M NaOH as a standard (quantum yield Φ = 0.90).[88,89] The lifetime values were obtained from the reconvolution fit analysis (Edinburgh F900 analysis software) of decay profiles obtained using the FLS920 instrument under excitation with a nitrogen-filled nanosecond flash-lamp. The quality of the fits was evidenced by the reduced χ^2 value ($\chi^2 < 1.1$).

Fluorescence anisotropy. Steady-state fluorescence anisotropies were measured using the Edinburgh Instruments FLS920 instrument, by inserting Glan–Thompson polarizers in the excitation and emission paths. Emission anisotropies were obtained at right angles using vertically polarized excitation light. Wavelength-dependent polarization correction factors (''*G*-factors'') were measured on the same sample under horizontally polarized excitation following standard procedures.

Two-photon absorption. Two-photon absorption cross sections (σ_2) were obtained from the two-photon excited fluorescence (TPEF) cross sections ($\sigma_2\Phi$) and the fluorescence emission quantum yield (Φ). TPEF cross sections in toluene (10^{-4} M chromophore concentration) were determined using a Ti-sapphire laser delivering 150 fs excitation pulses, according to the experimental protocol established by Xu and Webb.[90] This experimental protocol allows avoiding contributions from excited-state absorption that are known to result in largely overestimated TPA cross-sections. Fluorescein in 0.01 M NaOH, whose TPEF cross-sections are well-known,[90] served as the reference, taking into account the necessary corrections for the refractive index of the solvents.[91] The quadratic dependence of the fluorescence intensity on the excitation intensity was verified for each data point, indicating that the measurements were carried out in intensity regimes in which saturation or photodegradation do not occur. More details about the experimental setup have been previously published.[91]

Acknowledgements

F. T. acknowledges Université de Rennes 1 for an invited assistant professor position. We acknowledge financial support from CNRS, Région Bretagne (''Renouvellement des Compétences'' Program) and Rennes Métropole. Thanks are due to the Fundación Ramón Areces for a grant to A. Pla-Quintana.

References

1 R. R. Birge, *Acc. Chem. Res.*, 1986, **19**, 138–146.
2 S. Shima, R. P. Ilagan, N. Gillespie, B. J. Sommer, R. G. Hiller, F. P. Sharples, H. A. Frank and R. R. Birge, *J. Phys. Chem. A*, 2003, **107**, 8052–8066.
3 D. A. Parthenopoulos and P. M. Rentzepis, *Science*, 1989, **245**, 843–845.
4 J. H. Strickler and W. W. Webb, *Opt. Lett.*, 1991, **16**, 1780–1782.
5 A. S. Dvornikov and P. M. Rentzepis, *Opt. Commun.*, 1995, **119**, 341–346.
6 S. Maruo, O. Nakamura and S. Kawata, *Opt. Lett.*, 1997, **22**, 132–134.
7 B. H. Cumpston, S. P. Ananthavel, S. Barlow, D. L. Dyer, J. E. Ehrlich, L. L. Erskine, A. A. Heikal, S. M. Kuebler, I.-Y. S. Lee, D. McCord-Maughon, J. Qin, H. Röckel, M. Rumi, X. L. Wu, S. R. Marder and J. W. Perry, *Nature*, 1999, **398**, 51–54.
8 S. Kawata, H.-B. Sun, T. Tanaka and K. Takada, *Nature*, 2001, **412**, 697–698.
9 J. D. Bhawalkar, G. S. He, C.-K. Park, C. F. Zhao, G. Ruland and P. N. Prasad, *Opt. Commun.*, 1996, **124**, 33–37.
10 A. Abbotto, L. Beverina, R. Bozio, S. Bradamante, C. Ferrante, G. A. Pagani and R. Signorini, *Adv. Mater.*, 2000, **12**, 1963–1967.
11 W. Denk, J. H. Strickler and W. W. Webb, *Science*, 1990, **248**, 73–76.
12 C. Xu, W. Zipfel, J. B. Shear, R. M. Williams and W. W. Webb, *Proc. Natl. Acad. Sci. USA*, 1996, **93**, 10763–10768.
13 W. R. Zipfel, R. M. Williams, R. Christie, A. Y. Nikitin, B. T. Hyman and W. W. Webb, *Proc. Natl. Acad. Sci. USA*, 2003, **100**, 7075–7080.
14 J. D. Bhawalkar, N. D. Kumar, C. F. Zhao and P. N. Prasad, *J. Clin. Laser Med. Surg.*, 1997, **15**, 201–204.
15 G. S. He, J. D. Bhawalkar, C. F. Zhao and P. N. Prasad, *Appl. Phys. Lett.*, 1995, **67**, 2433–2435.
16 G. S. He, L. Yuan, N. Cheng, J. D. Bhawalkar, P. N. Prasad, L. L. Brott, S. J. Clarson and B. A. Reinhardt, *J. Opt. Soc. Am. B*, 1997, **14**, 1079–1087.
17 B. A. Reinhardt, L. L. Brott, S. J. Clarson, A. G. Dillard, J. C. Bhatt, R. Kannan, L. Yuan, G. S. He and P. N. Prasad, *Chem. Mater.*, 1998, **10**, 1863–1874.
18 K. D. Belfield, D. J. Hagan, E. W. Van Stryland, K. J. Schafer and R. A. Negres, *Org. Lett.*, 1999, **1**, 1575–1578.
19 Z.-q. Liu, Q. Fang, D. Wang, D.-x. Cao, G. Xue, W.-t. Yu and H. Lei, *Chem. Eur. J.*, 2003, **9**, 5074–5084.
20 S. Charier, O. Ruel, J.-B. Baudin, D. Alcor, J.-F. Allemand, A. Meglio and L. Jullien, *Angew. Chem., Int. Ed.*, 2004, **43**, 4785–4788.
21 G. S. He, G. C. Xu, P. N. Prasad, B. A. Reinhardt, J. C. Bhatt, R. McKellar and A. G. Dillard, *Opt. Lett.*, 1995, **20**, 435–437.

22 J. E. Ehrlich, X. L. Wu, I. Y. S. Lee, Z. Y. Hu, H. Röckel, S. R. Marder and J. W. Perry, *Opt. Lett.*, 1997, **22**, 1843–1845.
23 M. Albota, D. Beljonne, J.-L. Brédas, J. E. Ehrlich, J.-Y. Fu, A. A. Heikal, S. E. Hess, T. Kogej, M. D. Levin, S. R. Marder, D. McCord-Maughon, J. W. Perry, H. Röckel, M. Rumi, G. Subramaniam, W. W. Webb, X.-L. Wu and C. Xu, *Science*, 1998, **281**, 1653–1656.
24 L. Ventelon, L. Moreaux, J. Mertz and M. Blanchard-Desce, *Chem. Commun.*, 1999, 2055–2056.
25 O.-K. Kim, K.-S. Lee, H. Y. Woo, K.-S. Kim, G. S. He, J. Swiatkiewicz and P. N. Prasad, *Chem. Mater.*, 2000, **12**, 284–286.
26 L. Ventelon, S. Charier, L. Moreaux, J. Mertz and M. Blanchard-Desce, *Angew. Chem., Int. Ed.*, 2001, **40**, 2098–2101.
27 P. K. Frederiksen, M. Jørgensen and P. R. Ogilby, *J. Am. Chem. Soc.*, 2001, **123**, 1215–1221.
28 O. Mongin, L. Porrès, L. Moreaux, J. Mertz and M. Blanchard-Desce, *Org. Lett.*, 2002, **4**, 719–722.
29 A. Abbotto, L. Beverina, R. Bozio, A. Facchetti, C. Ferrante, G. A. Pagani, D. Pedron and R. Signorini, *Org. Lett.*, 2002, **4**, 1495–1498.
30 W. J. Yang, D. Y. Kim, M.-Y. Jeong, H. M. Kim, S.-J. Jeon and B. R. Cho, *Chem. Commun.*, 2003, 2618–2619.
31 M. H. V. Werts, S. Gmouh, O. Mongin, T. Pons and M. Blanchard-Desce, *J. Am. Chem. Soc.*, 2004, **126**, 16294–16295.
32 K. D. Belfield, A. R. Morales, B.-S. Kang, J. M. Hales, D. J. Hagan, E. W. Van Stryland, V. M. Chapela and J. Percino, *Chem. Mater.*, 2004, **16**, 4634–4641.
33 Z.-Q. Liu, Q. Fang, D.-X. Cao, D. Wang and G.-B. Xu, *Org. Lett.*, 2004, **6**, 2933–2936.
34 S. K. Lee, W. J. Yang, J. J. Choi, C. H. Kim, S.-J. Jeon and B. R. Cho, *Org. Lett.*, 2005, **7**, 323–326.
35 S.-J. Chung, M. Rumi, V. Alain, S. Barlow, J. W. Perry and S. R. Marder, *J. Am. Chem. Soc.*, 2005, **127**, 10844–10845.
36 H. Y. Woo, B. Liu, B. Kohler, D. Korystov, A. Mikhailovsky and G. C. Bazan, *J. Am. Chem. Soc.*, 2005, **127**, 14721–14729.
37 V. Strehmel, A. M. Sarker, P. M. Lahti, F. E. Karasz, M. Heydenreich, H. Wetzel, S. Haebel and B. Strehmel, *ChemPhysChem*, 2005, **6**, 267–276.
38 O. Mongin, L. Porrès, M. Charlot, C. Katan and M. Blanchard-Desce, *Chem. Eur. J.*, 2007, **13**, 1481–1498.
39 M. P. Joshi, J. Swiatkiewicz, F. Xu, P. N. Prasad, B. A. Reinhardt and R. Kannan, *Opt. Lett.*, 1998, **23**, 1742–1744.
40 S.-J. Chung, K.-S. Kim, T.-C. Lin, G. S. He, J. Swiatkiewicz and P. N. Prasad, *J. Phys. Chem. B*, 1999, **103**, 10741–10745.
41 G. S. He, J. Swiatkiewicz, Y. Jiang, P. N. Prasad, B. A. Reinhardt, L.-S. Tan and R. Kannan, *J. Phys. Chem. A*, 2000, **104**, 4805–4810.
42 B. R. Cho, K. H. Son, S. H. Lee, Y.-S. Song, Y.-K. Lee, S.-J. Jeon, J. H. Choi, H. Lee and M. Cho, *J. Am. Chem. Soc.*, 2001, **123**, 10039–10045.
43 D. Beljonne, W. Wenseleers, E. Zojer, Z. Shuai, H. Vogel, S. J. K. Pond, J. W. Perry, S. R. Marder and J.-L. Brédas, *Adv. Funct. Mater.*, 2002, **12**, 631–641.
44 A. Adronov, J. M. J. Fréchet, G. S. He, K.-S. Kim, S.-J. Chung, J. Swiatkiewicz and P. N. Prasad, *Chem. Mater.*, 2000, **12**, 2838–2841.
45 S.-J. Chung, T.-C. Lin, K.-S. Kim, G. S. He, J. Swiatkiewicz, P. N. Prasad, G. A. Baker and F. V. Bright, *Chem. Mater.*, 2001, **13**, 4071–4076.
46 A. Abbotto, L. Beverina, R. Bozio, A. Facchetti, C. Ferrante, G. A. Pagani, D. Pedron and R. Signorini, *Chem. Commun.*, 2003, 2144–2145.
47 O. Mongin, L. Porrès, C. Katan, T. Pons, J. Mertz and M. Blanchard-Desce, *Tetrahedron Lett.*, 2003, **44**, 8121–8125.
48 J. Yoo, S. K. Yang, M.-Y. Jeong, H. C. Ahn, S.-J. Jeon and B. R. Cho, *Org. Lett.*, 2003, **5**, 645–648.
49 L. Porrès, O. Mongin, C. Katan, M. Charlot, T. Pons, J. Mertz and M. Blanchard-Desce, *Org. Lett.*, 2004, **6**, 47–50.
50 C. Katan, F. Terenziani, O. Mongin, M. H. V. Werts, L. Porrès, T. Pons, J. Mertz, S. Tretiak and M. Blanchard-Desce, *J. Phys. Chem. A*, 2005, **109**, 3024–3037.
51 C. Le Droumaguet, O. Mongin, M. H. V. Werts and M. Blanchard-Desce, *Chem. Commun.*, 2005, 2802–2804.
52 M. Drobizhev, A. Karotki, A. Rebane and C. W. Spangler, *Opt. Lett.*, 2001, **26**, 1081–1083.
53 M. Drobizhev, A. Karotki, Y. Dzenis, A. Rebane, Z. Suo and C. W. Spangler, *J. Phys. Chem. B*, 2003, **107**, 7540–7543.
54 O. Mongin, J. Brunel, L. Porrès and M. Blanchard-Desce, *Tetrahedron Lett.*, 2003, **44**, 2813–2816.
55 O. Varnavski, X. Yan, O. Mongin, M. Blanchard-Desce and T. Goodson, III, *J. Phys. Chem. C*, 2007, **111**, 149–162.
56 Corresponding to the combination of reduced absorption and scattering.
57 In relation with reduced excitation of endogenous chromophores.
58 D. R. Larson, W. R. Zipfel, R. M. Williams, S. W. Clark, M. P. Bruchez, F. W. Wise and W. W. Webb, *Science*, 2003, **300**, 1434–1437.
59 X. Michalet, F. F. Pinaud, L. A. Bentolila, J. M. Tsay, S. Doose, J. J. Li, G. Sundaresan, A. M. Wu, S. S. Gambhir and S. Weiss, *Science*, 2005, **307**, 538–544.
60 R. Hardman, *Environ. Health Perspect.*, 2006, **114**, 165–172.
61 O. Mongin, T. R. Krishna, M. H. V. Werts, A.-M. Caminade, J.-P. Majoral and M. Blanchard-Desce, *Chem. Commun.*, 2006, 915–917.
62 Phosphorus dendrimers have been shown to have low toxicity, see: M. Maszewska, J. Leclaire, M. Cieslak, B. Nawrot, A. Okruszek, A.-M. Caminade and J.-P. Majoral, *Oligonucleotides*, 2003, **13**, 193–205.
63 W. West and S. Pearce, *J. Phys. Chem.*, 1965, **69**, 1894–1903.
64 G. De Belder, G. Schweitzer, S. Jordens, M. Lor, S. Mitra, J. Hofkens, S. De Feyter, M. Van der Auweraer, A. Herrmann, T. Weil, K. Müllen and F. C. De Schryver, *ChemPhysChem*, 2001, **2**, 49–55.
65 F. Terenziani, M. Morone, S. Gmouh and M. Blanchard-Desce, *ChemPhysChem*, 2006, **7**, 685–696.
66 G. D'Avino, F. Terenziani and A. Painelli, *J. Phys. Chem. B*, 2006, **110**, 25590–25592.
67 J.-P. Majoral and A.-M. Caminade, *Chem. Rev.*, 1999, **99**, 845–880.
68 A.-M. Caminade and J.-P. Majoral, *Acc. Chem. Res.*, 2004, **37**, 341–348.
69 A.-M. Caminade and J.-P. Majoral, *Prog. Polym. Sci.*, 2005, **30**, 491–505.
70 N. Launay, A.-M. Caminade and J. P. Majoral, *J. Organomet. Chem.*, 1997, **529**, 51–58.
71 T. R. Krishna, M. Parent, M. H. V. Werts, L. Moreaux, S. Gmouh, S. Charpak, A.-M. Caminade, J.-P. Majoral and M. Blanchard-Desce, *Angew. Chem., Int. Ed.*, 2006, **45**, 4645–4648.
72 A slight apparent decrease of the effective absorption coefficient per chromophore is observed for dendrimers **G3** and **G4** (inferior to that of reference fluorophore **F**) This is most probably an artifact related to the presence of an increasing amount of solvent molecules trapped in the dendrimer interior. A similar effect is consequently observed for the maximum TPA cross-section of **G3** and **G4**.
73 F. Terenziani, A. Painelli, C. Katan, M. Charlot and M. Blanchard-Desce, *J. Am. Chem. Soc.*, 2006, **128**, 15742–15755.
74 M. N. Berberan-Santos, J. Pouget, B. Valeur, J. Canceill, L. Jullien and J. M. Lehn, *J. Phys. Chem.*, 1993, **97**, 11376–11379.
75 T. Pullerits and V. Sundström, *Acc. Chem. Res.*, 1996, **29**, 381–389.
76 R. van Grondelle, R. Monshouwer and L. Valkunas, *Pure Appl. Chem.*, 1997, **69**, 1211–1218.
77 E. K. L. Yeow, K. P. Ghiggino, J. N. H. Reek, M. J. Crossley, A. W. Bosman, A. P. H. J. Schenning and E. W. Meijer, *J. Phys. Chem. B*, 2000, **104**, 2596–2606.
78 M. Maus, S. Mitra, M. Lor, J. Hofkens, T. Weil, A. Herrmann, K. Mullen and F. C. De Schryver, *J. Phys. Chem. A*, 2001, **105**, 3961–3966.
79 J. Larsen, J. Andersson, T. Polivka, J. Sly, M. J. Crossley, V. Sundström and E. Akesson, *Chem. Phys. Lett.*, 2005, **403**, 205–210.
80 Time-resolved fluorescence anisotropy decay measurements study on dendrimers **G1–G4** indicates that this energy transfer is indeed very fast: M. Guo and T. Goodson, III, personal communication.
81 T. Förster, *Ann. Phys.*, 1948, **2**, 55–75.
82 A decrease of the fluorescence quantum yield accompanied by the appearance of an emission tail at lower energy has also been observed in dendrimers decorated with naphthyl units: F. Pina, P. Passaniti, M. Maestri, V. Balzani, F. Vögtle, M. Gorka, S.-K. Lee, J. Van Heyst and H. Fakhrnabavi, *ChemPhysChem*, 2004, **5**, 473–480.

83 Model chromophore **F** exhibits an anisotropy of 0.18, and reference monochromophoric compounds **C0** and **C1** display values of 0.22 and 0.28, respectively. Since these two dendrimer-embedded chromophores differ only in generation number, the increase in anisotropy value can be related to the slowing-down of the rotational diffusion for increasing molecule size.
84 DOND **G′0** shows the smaller anisotropy value at low wavelength (0.07), which might indicate that energy transfer from core chromophore to peripheral ones also takes place in that case (in relation with the smaller distance between core and peripheral chromophores). Wavelength-dependent time-resolved anisotropy measurements are required to derive final conclusion.
85 The fluorescence quantum yield is an effective value since both the core and peripheral chromophores contribute to emission. Its value is thus expected to depend on the excitation wavelength, which controls the relative contribution (in addition to the relative number of chromophores) of excitation of each type of chromophores. The values given in Table 1 correspond to excitation at the absorption maximum.
86 Except for dendrimer **G′2** that shows slightly higher TPA cross-sections.
87 Even if their PL characteristics show that emitting fluorophores of SOND dendrimers experience a more polar environment, the average TPA response of the decorating fluorophores is similar to that of an isolated molecule (Fig. 12), which was also the case for one-photon absorption (Fig. 4).
88 J. N. Demas and G. A. Crosby, *J. Phys. Chem.*, 1971, **75**, 991–1024.
89 D. F. Eaton, *Pure Appl. Chem.*, 1988, **60**, 1107–1114.
90 C. Xu and W. W. Webb, *J. Opt. Soc. Am. B*, 1996, **13**, 481–491.
91 M. H. V. Werts, N. Nerambourg, D. Pélégry, Y. Le Grand and M. Blanchard-Desce, *Photochem. Photobiol. Sci.*, 2005, **4**, 531–538.